Recovery of harmonic-like behavior of the polar mode in $BaTiO_3$ at high pressures

A. Herlihy,[1,2] T. A. Bird,[1] C. J. Ridley,[2] C. L. Bull,[2,3] N. P. Funnell,[2,*] and M. S. Senn[1,†]

[1]*Department of Chemistry, University of Warwick, Gibbet Hill, Coventry, CV4 7AL, United Kingdom*

[2]*ISIS Neutron and Muon Facility, Rutherford Appleton Laboratory, Didcot, OX11 0QX, United Kingdom*

[3]*School of Chemistry, University of Edinburgh, David Brewster Road, Edinburgh, EH9 3FJ, United Kingdom*

(Received 29 November 2021; revised 7 February 2022; accepted 16 February 2022; published 28 March 2022)

The local structure of high-pressure $BaTiO_3$ has been interrogated by neutron total scattering methods up to pressures of 4.18 GPa at ambient temperature. Competitive refinements of cubic, tetragonal, and rhombohedral distortion modes against pair distribution functions indicate contrasting local structure behavior of temperature- and pressure-induced cubic $BaTiO_3$. Suppression of the mode amplitude, isotropy of the order-parameter direction, and loss of sensitivity to correlated Ti displacements at high pressure all suggest a high-pressure local structure that is more consistent with the harmonic approximation rather than an order-disorder model which better describes high-temperature cubic $BaTiO_3$ in the vicinity of the tetragonal phase transition.

DOI: 10.1103/PhysRevB.105.094114

I. INTRODUCTION

$BaTiO_3$ is often given as a classic example of a proper ferroelectric where, due to the second-order Jahn-Teller effect, off-centering of the Ti^{4+} cation from its TiO_6 octahedron results in a net polarization [1]. The resulting ferroelectric properties and high dielectric constant make $BaTiO_3$ a very attractive material for use in devices such as capacitors [2], and the perovskite-structured material [shown in Figure 1(a)] has become the prototypical ferroelectric intensively studied to understand the link between ferroelectricity and crystal structure. Despite many decades of investigation, there remains an ongoing debate about the nature of the ferroelectric phase transition. Above its Curie temperature (T_C), $BaTiO_3$ adopts a cubic structure. Below T_C, the structure is reduced to a tetragonal symmetry and on decreasing temperature further, $BaTiO_3$ transforms to an orthorhombic and, finally, to a rhombohedral structure [3–6].

A popular theory, suggested by Cochran [5], describes a displacive model whereby Ti^{4+} cations are displaced microscopically along ⟨100⟩, ⟨110⟩, and ⟨111⟩ directions for the tetragonal, orthorhombic, and rhombohedral phases, respectively. This model, however, fails to address key observations such as the strong diffuse x-ray scattering in all but the rhombohedral phase [7–9] and the presence of first-order Raman excitations in the cubic phase [10]. In 1968, Comés *et al.* [7] proposed an order-disorder (OD) model, also commonly referred to as the "eight-site" model, where the crystallographically rich phase diagram of $BaTiO_3$ is rationalized due to correlations of local Ti displacements along the eight ⟨111⟩ directions. Correlated displacements of the Ti atom in successive ⟨100⟩ directions give rise to the observed average symmetry, and it is this underlying disorder that appears to simultaneously reconcile the perceived average symmetry with the anomalous experimental results, discussed above.

Since the first proposal of these two contending models, a multitude of experimental and computational studies have favored either one of these two possible scenarios. Local probes tend to support an OD model [11–13]; for example, our symmetry-motivated analyses of pair distribution functions (PDFs) of $BaTiO_3$ have shown that Ti displacements are rhombohedral-like across all known phases [14]. However, the observation of heavily damped modes [15–17] appears at odds with an OD model and supports the soft-mode explanation. Furthermore, there is not yet consensus—within the OD interpretation—on the exact nature of the disordered local arrangements of Ti cations, where some reports via solid-state NMR [12] suggest a local tetragonal distortion and others support a rhombohedral [11,18] distortion.

More recently, additional work has come out in support of the soft-mode model [9], where diffuse scattering is attributed to the overdamped anharmonic soft phonon branch. This results in a local probability distribution for the Ti atoms that has a minimum coinciding with the average crystallographic position and a maximum along ⟨111⟩ directions with an average magnitude of ca. 0.15 Å. It seems that a wealth of experimental and computational observations can either be explained by invoking an OD scenario or by considering highly overdamped, anharmonic, soft phonon modes that imply the Ti atoms spend a substantial amount of time off center. Regardless of the perspective adopted, it is clear that the local symmetry deviates substantially from the average crystallographic symmetry over short length scales and long time periods, indicating a significant departure from the harmonic

*nick.funnell@stfc.ac.uk
†m.senn@warwick.ac.uk

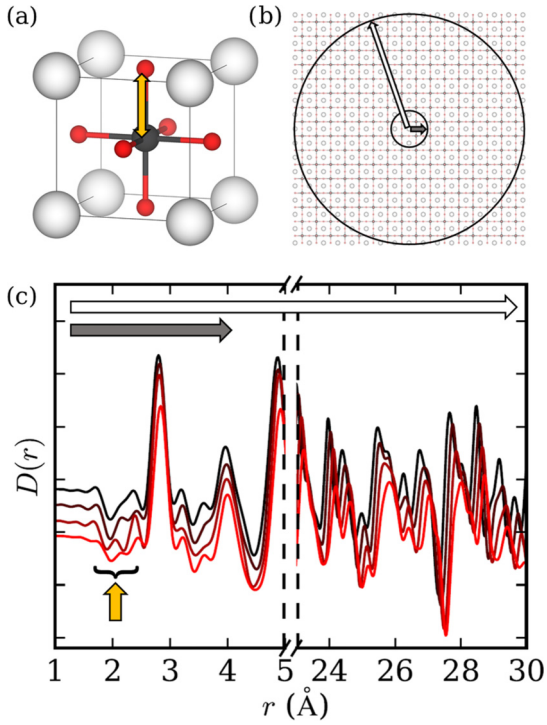

FIG. 1. (a) The average structure unit cell of cubic $BaTiO_3$ with an arrow indicating the shortest atom–atom correlation within the structure (Ti–O). (b) The longer-range structure and circles with radii of 4 and 30 Å indicating the minimum and maximum range of atom–atom correlations probed by our variable range PDF refinements. (c) Variable-pressure PDFs measured on PEARL (offset in the y-direction with increasing pressure for clarity). The yellow arrow indicates the features arising due to the Ti–O correlations and the horizontal arrows correspond to the probe distances shown in (b).

soft-mode/displacive picture. Consideration of the long-range ordering of dynamic ⟨111⟩ Ti displacements projected onto the ⟨100⟩ directions appears to reconcile these two models [14].

Clearly the investigation of the temperature-induced phase transitions of $BaTiO_3$ has been extensive, and a wide range of techniques have been utilized to investigate the average and local structure of the perovskite material [19]. However, challenges associated with *in situ* high-pressure measurements have perhaps limited investigation of the local structure of $BaTiO_3$ in other regions of the phase diagram.

It is predicted that modest hydrostatic pressure will initially act to suppress ferroelectric distortions in ABO_3 perovskites due to the increasing influence of short-range electronic repulsions over long-range Coulomb ionic interactions which favor polar distortions [20]. This is borne out by the well-established average structure phase diagram of $BaTiO_3$ that indicates that at ambient temperature, there is a tetragonal-to-cubic phase transition at ca. 2 GPa [6,21,22]. However, high-pressure Raman studies show evidence for persistent disorder within the cubic phase, with the suggestion that this disorder results from off-center Ti atoms and grain boundary/intergrain stress [23]. X-ray absorption spectroscopy (XAS) of the Ti *K* edge also suggests that Ti remains displaced until 10 GPa, above which the Ti is centered, and local and average symmetries are reconciled [24]. Together, these results might imply that the high-temperature and high-pressure behaviors mimic each other from both an average (crystallographic) and local structure perspective. However, neither of these studies appears to have allowed for robust refinement of models with competing symmetries against the local probe data.

On the other hand, PDFs generated from total scattering experiments and their sensitivity to short-range atom–atom correlations are well suited to this kind of modeling that interrogates the precise local symmetry-breaking behavior in $BaTiO_3$. While x-ray PDF work has been carried out [25], the insensitivity of x-rays to the lighter oxygen atoms often fails to resolve the level of detail available to neutron measurements. The lack of high-pressure neutron PDF studies of $BaTiO_3$ and indeed of crystalline materials more generally can be attributed to the often opposing requirements of high-pressure and PDF experiments. It is only relatively recently that high-pressure neutron PDF measurements have been achieved for crystalline materials [26,27].

With this in mind, we undertake the first analysis of neutron total scattering measurements of $BaTiO_3$ at pressures up to 4.2 GPa in order to directly investigate the nature of the pressure-induced tetragonal-to-cubic phase transition of $BaTiO_3$ over a range of length scales. Building on our recently developed symmetry-adapted PDF analysis (SAPA) [28] technique, whereby distortion modes grouped by irreducible representation are refined against local structure measurements, we analyze the high-pressure PDF data, revealing pressure-induced suppression of the local Ti displacements. We apply the same modeling approach to previously published variable temperature PDFs [14] in order to determine how the departure of local from average symmetry compares for pressure versus temperature. Our analysis of ambient temperature, variable pressure PDFs points toward a gradual pressure-induced suppression of the anharmonic potential implicit in describing the OD behavior of $BaTiO_3$, toward a more harmonic-like potential, more consistent with a soft-mode picture.

II. EXPERIMENTAL DETAILS AND DATA ANALYSIS

Polycrystalline $BaTiO_3$ (also used for the variable-temperature study described in Ref. [14]) was measured [29] on the high-pressure instrument PEARL [30] at the ISIS Neutron and Muon Facility. The powder sample was loaded into a null-scattering Ti–Zr single-toroidal gasket, with a gas loader [31], used to fill the remaining gasket volume with an argon gas pressure transmitting media (PTM). A Paris–Edinburgh (PE) press, equipped with zirconia-toughened alumina (ZTA) anvils, was used to apply loads of 3, 25, 40, and 50 tonnes to the sample. The lattice parameters of $BaTiO_3$ were determined from Rietveld refinement against the Bragg data and the known equation of state [22] used to calculate sample pressures of 0.24(2), 1.19(2), 2.55(6), and 4.18(8) GPa. Neutron powder diffraction patterns were collected for a minimum of 11 h each to ensure sufficient signal-to-noise ratio at high Q (where $Q = (4\pi \sin\theta)/\lambda$). Stacked vanadium discs were measured in the same way with an argon PTM, and analogous data collections were performed at loads of 8, 20, 30, and

45 tonnes corresponding to pressures roughly equivalent to those of the measured $BaTiO_3$ data. Total scattering data were collected and treated using the same procedure described in Refs. [26] and [27] without the added complication of needing to model the PTM, since argon gas is a relatively weak neutron scatterer. A low-intensity peak at 4.18 GPa was tentatively indexed as the (111) reflection of solid argon. However, there was no evidence of an argon contribution to the PDF (i.e., no misfits in regions where an Ar–Ar peak would be expected).

Data were reduced using the MANTID software package [32] to correct for the effects of attenuation by the ZTA anvils and normalized by a vanadium standard to account for flux profile and detector efficiencies. Contaminant pairwise correlations, arising from components of the PE press (notably alumina from the anvils), were accounted for by performing a separate set of container measurements, where a vanadium sample was compressed in an analogous setup to the $BaTiO_3$ sample. Load was progressively increased such that comparable gasket geometry seen at each sample pressure was produced. All the same contaminant species were present and these were subtracted from the $BaTiO_3$ measurements. Total scattering patterns [$S(Q)$s] were produced by applying scaling and offset values such that $S(Q) \rightarrow 1$ at Q_{max}. PDFs [shown in Fig. 1(c)] were obtained via Fourier transform of the $S(Q)$ function using the program STOG distributed with the RMCPROFILE package [33].

PDF modeling and Rietveld refinements were carried out using TOPAS ACADEMIC software v6 [34]. We performed small-box variable range PDF refinements [19,35] with the minimum of the fitting range (r_{min}) kept constant at 1.2 Å, and the maximum (r_{max}) varied from 4 to 30 Å in steps of 1 Å. Therefore, the overall fitting range was varied between 2.8 and 28.8 Å, such that increasingly large length-scale atom–atom correlations were probed with increasingly large r_{max} values, as depicted in Fig. 1(b). This is in contrast to so-called "box-car" refinements [36,37] where the fitting range is held constant and shifted along the PDF, resulting in the progressively reduced influence of the immediate local structure on the refined small-box model. We used a $P1$ unit cell, refining only the polar distortion modes associated with Ti and O which transform as the Γ_4^- irreducible representation (irrep) and fixing Ba modes to zero to avoid a floating origin of the unit cell. The most general order-parameter direction (OPD) associated with this irrep is three dimensional (a, b, c). The Ti(T_{1u}), O(A_{2u}), and O(E_u) modes that form a basis of this irrep thus have three branches each where particular constraints on the branched mode amplitudes correspond to higher symmetry OPDs.

Rather than allowing distortion modes to refine freely, we constrained the OPD to be consistent with cubic (0,0,0), tetragonal (a,0,0), and rhombohedral (a,a,a) symmetries (Fig. 2) in order to test these three specific local distortion behaviors. We did not consider other order parameters such as (a,a,0), (a,b,0), or (a,a,b) as the aim of this work was to resolve the OD behavior of $BaTiO_3$ at the tetragonal to cubic phase transition. We found that unconstrained refinements of the Ti(T_{1u}), O(A_{2u}), and O(E_u) modes resulted in nonphysical coupling, particularly for refinements of the PDFs measured at 2.55 and 4.18 GPa where for r_{max} values of greater than 10 Å,

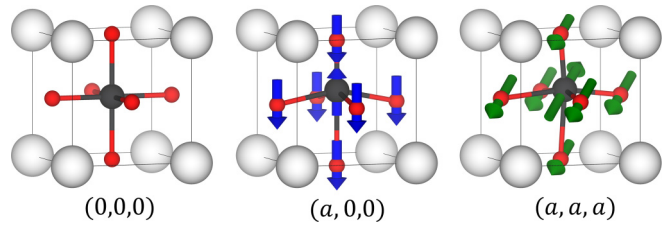

FIG. 2. Schematic representation of the $|Q(\Gamma_4^-)|$ mode showing the collective and relative displacements of the Ti and O atoms with the OPD indicated below each representation, corresponding to cubic-, tetragonal-, and rhombohedral-type displacements, respectively.

Ti and O atoms refined to displace in the same, rather than opposite, directions (see Supplemental Material [38]). In order to maintain the correct relative displacements associated with the modes, a ratio of $1 : -1.6 : -1.3$ for Ti(T_{1u}):O(A_{2u}):O(E_u) displacements, respectively, was applied. These values were calculated by averaging ratios determined by fitting rhombohedral (a,a,a) models against high-quality diffraction data measured at 15 and 293 K on the GEM instrument, previously [14]. Mode amplitude values reported herein refer to the A_P values defined in ISODISTORT [39], as the parent-cell-normalized amplitude, and are assigned the mode-specific notation $|Q(\Gamma_4^-)|$. We found that although the refined $|Q(\Gamma_4^-)|$ values differ slightly depending on the precise ratio used, the relative values and fitting statistics of each refinement remain essentially constant. Lattice parameters determined from Rietveld refinements of the diffraction patterns (see Supplemental Material [38]) were fixed for all small-box PDF refinements, constraining the metric symmetries to those known from the average structures. The *beq_r_r2* function (discussed further in Ref. [28]) was used to describe the correlated thermal motion that leads to r-dependent broadening, with isotropic displacement parameters fixed to the lower limits found for the three models (see Supplemental Material [38] for further details). The sensitivity of our modeling approach to the limited Q_{max} (20.32 $Å^{-1}$) available on PEARL was thoroughly investigated and reported within the Appendix.

III. RESULTS AND DISCUSSION

Neutron-diffraction patterns indicate that the measured average structure of $BaTiO_3$ at variable pressure is consistent with previous literature [6,22,40]. The neutron-diffraction patterns (see Supplemental Material [38]) at 0.24 and 1.19 GPa exhibited clear peak splitting [particularly the (200)/(002) reflection], indicative of a tetragonal symmetry, and Rietveld refinements confirmed a $P4\,mm$ average crystal structure. Above 2 GPa, $BaTiO_3$ goes through a well-documented phase transition to an average cubic symmetry ($Pm\bar{3}m$), confirmed again by Rietveld refinement at 2.55 and 4.18 GPa.

Refining small-box models over an increasing range of the PDF provides information on the correlation length scale. This is particularly relevant for materials with OD behavior such as $BaTiO_3$ where a local rhombohedral distortion may be observed over a short length scale, for example, one unit cell; however, longer length scales will increasingly resemble the

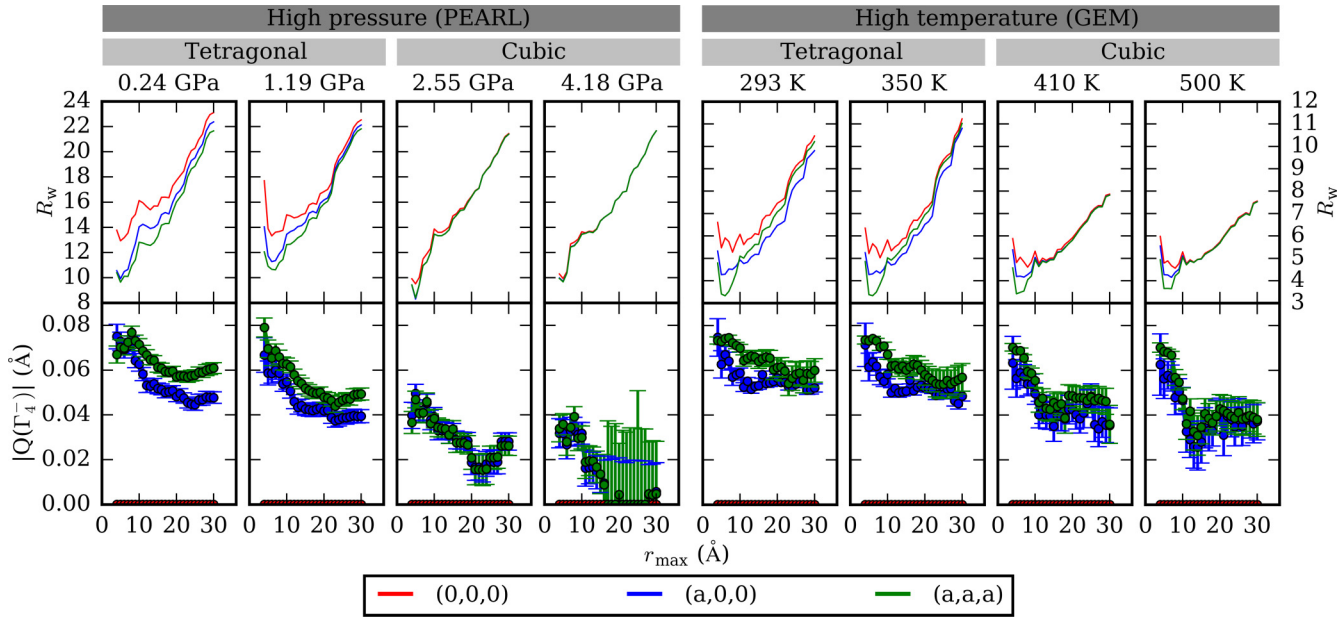

FIG. 3. R_w and $|Q(\Gamma_4^-)|$ values for variable range refinements for cubic (0,0,0), tetragonal (a,0,0), and rhombohedral (a,a,a) OPDs against variable pressure (left) and temperature (right) PDFs. $|Q(\Gamma_4^-)|$ values for the cubic model were fixed at zero. R_w values for tetragonal and rhombohedral modes in the high-pressure cubic data are almost exactly coincident and cannot be visually distinguished.

average structure. Comparisons of fitting statistics (R_w) and $|Q(\Gamma_4^-)|$ values (shown in Fig. 3) for cubic, tetragonal, and rhombohedral models provide insight into the evolution of local displacements of Ti and O atoms as a function of pressure. We demonstrate that even for the limited Q_{max} available on PEARL, our data are sensitive to subtle changes in the local structure (see the Appendix).

We compare our findings for the local structure of $BaTiO_3$ at high pressure with analogous results for the thermally induced phase transition. The same modeling approach has been applied to PDFs measured at 293, 350, 410, and 500 K using the GEM instrument at ISIS (and processed with a Q_{max} of 20 $Å^{-1}$ for a fairer comparison) and previously published in support of persistent OD behavior at high temperature [14]. The average structure of $BaTiO_3$ is tetragonal at 293 and 350 K and cubic at 410 and 500 K, inviting a comparison of the local structure of $BaTiO_3$ at high pressure and high temperature.

At 0.24 and 1.19 GPa consistent improvements in R_w over all r_{max} (shown in Fig. 3) indicate that the local and medium-range structure of $BaTiO_3$ is best described by a rhombohedral displacement of the Ti atom. The refined $|Q(\Gamma_4^-)|$ values for an (a,0,0) OPD are approximately $\sqrt{3}/2$ smaller than those of an (a,a,a) OPD suggesting that we are essentially resolving a projection of the [111] type displacement onto the [100] direction.

The results for the local structure of $BaTiO_3$ at 1.19 GPa are essentially very similar to those found for the structure at 0.24 GPa and a decrease in $|Q(\Gamma_4^-)|$ of ca. 15% points toward a small pressure-induced hardening of the local potential describing the off-center displacements. These results are comparable with those of the variable temperature PDFs measured at 293 and 350 K. R_w values at 293 and 350 K again favor the rhombohedral-type displacements up to $r_{max} = 10$ Å, after which fitting statistics favor the tetragonal model, indicating sensitivity of the PDF to the average, long-range structure. $|Q(\Gamma_4^-)|$ values are in good agreement with the variable pressure results. Again, relative $|Q(\Gamma_4^-)|$ values for (a,0,0) compared with (a,a,a) OPDs suggest the resolution of the [111] type displacement onto the [100] direction.

Results for high-pressure cubic $BaTiO_3$ point toward a departure from the local structure behavior of the high-pressure tetragonal phase and perhaps more interestingly from the local structure of the high-temperature cubic phase. At 2.55 and 4.18 GPa, $|Q(\Gamma_4^-)|$ at $r_{max} = 4$ Å becomes suppressed by ca. 1/2 (cf. 0.24 GPa) and the magnitudes of $|Q(\Gamma_4^-)|$ with OPD (a,0,0) and (a,a,a) are approximately equal. Over all r_{max} there is a negligible difference between the R_w values for models with tetragonal and rhombohedral Ti displacements. At 2.55 GPa the difference between cubic models and models with off-center displacements decreases approximately linearly until $r_{max} = 20$ Å, after which the difference in R_w drops below significance, whereas at 4.18 GPa this occurs at $r_{max} = 10$ Å. At 4.18 GPa, by 16 Å, $|Q(\Gamma_4^-)|$ refines to zero, suggesting that the correlation length of the Ti displacements is below four unit cell lengths. The suppression of $|Q(\Gamma_4^-)|$, isotropy of the displacement with respect to the different OPD, and the reduction in correlation lengths are all consistent with the ferroelectric instability in $BaTiO_3$ being well described by the harmonic approximation at elevated pressures.

On the other hand, our results regarding previously published high-temperature PDF data clearly favor an (a,a,a) OPD, consistent with the model of chains of rhombohedrally displaced off-center Ti atoms, which retain substantial correlations along ⟨100⟩ directions. At 410 and 500 K, refined $|Q(\Gamma_4^-)|$ values over $r_{max} = 4$–10 Å) are similar to those observed at lower temperatures (at $r_{max} = 4$ Å, $|Q(\Gamma_4^-)|$ at 293 K

= 0.094 Å, 350 K = 0.074 Å, 410 K = 0.071 Å, 500 K = 0.071 Å) but drop to values that are ca. 2/3 of those observed over longer r_{max}. The persisting sensitivity to off-center displacements in the high-temperature cubic regime is consistent with the model of correlated chains of [111] displacements projected along the [100] axis and lends further support to the OD model for the temperature-induced phase transition.

We find that our observed high-pressure trends of the local structure agree with the work of Ravy *et al.* [8] who report diminishing diffuse scattering planes at high pressure and broadening of the diffuse features indicative of a decrease in correlation length of Ti chains, which they discuss in the wider context of pressure-induced Ti centering. Correlation lengths of ca. six unit cell lengths (ca. 24 Å) implied by broadened diffuse features at ca. 4 GPa are also in good agreement with our results, where diffuse scattering is sensitive to chain correlations and the PDF method will average chain and nonchain interactions. While the reported diffuse scattering is sensitive to chain correlations, it is less sensitive to the precise nature of the local symmetry breaking. On the other hand, the method we report here for analyzing our high-pressure PDFs has a higher degree of sensitivity to the local symmetry breaking at low r_{max} but will average over chain and nonchain interactions at high r_{max}, and thus the two approaches should be viewed as providing complementary information.

We stress that although XAS measurements suggest continual off-center Ti displacements up to 10 GPa [24], the sensitivity of the technique is limited to the immediate local environment of the probe atom, extending as far as the next-nearest neighbor only. This makes it difficult to judge how these results differ from those expected from the root-mean-square displacement of a harmonic oscillator—estimated to be 0.05 Å at 4.18 GPa from our r_{max} = 4 Å refinements (see Fig. 3).

It is perhaps interesting to speculate on the differing local structure behavior of high-temperature and high-pressure $BaTiO_3$. Given that polar distortions are in general coupled to the expansion of the lattice, it is understandable that the application of pressure will act to reduce the magnitude of the Ti and O displacements until they are consistent with those expected within the harmonic approximation in which displacements along [111], [100], or indeed any other lattice direction necessarily carry the same energy penalty. On the other hand, above the tetragonal to cubic phase transition positive thermal lattice expansion dominates and no resulting hardening of the anharmonic potential that describes the Ti off centering is observed.

Our results not only show robustly that the OD behavior of $BaTiO_3$ is suppressed at high pressure but also add to an emerging research direction on neutron local structure measurements of crystalline materials under hydrostatic pressure [26,27], where local structure analysis approaches such as the symmetry-motivated approach we have used here can be applied. Such experiments would provide fundamental insight into the pressure-induced mode softening in negative thermal expansion materials like ScF_3 [41,42], for example, or pressure-induced phase behavior of framework materials such as Prussian blue analogues [43,44].

IV. CONCLUSION

Although it might be tempting to conclude from the average structures that the high-temperature and high-pressure tetragonal and cubic phases behave in an analogous way, in terms of the local structure, our detailed high-pressure PDF study shows that this is not the case. Our symmetry-motivated approach of interrogating the local structure of $BaTiO_3$ reveals that at high pressure, the OD model provides a less satisfactory description. By 2.55 GPa already, significant suppression of the mode amplitude over short r_{max}, isotropy of the OPD and loss of sensitivity to correlated Ti displacements at high pressure all point toward a more harmonic character of the polar mode which contrasts the high-temperature behavior.

ACKNOWLEDGMENTS

We thank Prof. D. Keen for supplying the total scattering data from GEM. A.H. thanks the Science and Technology Facilities Council and the University of Warwick for a studentship. M.S.S. acknowledges the Royal Society for a University Research Fellowship (UF160265) and the EPSRC for funding (EP/S027106/1). We are grateful to STFC for the provision of neutron beam time at ISIS supported under experiment number RB1910162 [29].

APPENDIX: VALIDATION OF PDF SENSITIVITY

In order to evaluate the sensitivity of our modeling approach to limited Q_{max} values of the PEARL data, PDFs were processed from room temperature $S(Q)$s measured on GEM, from Ref. [14] with artificially lowered Q_{max} values of 10–40 $Å^{-1}$ in steps of 5 $Å^{-1}$. A rhombohedral model was fit to this contiguous series of PDFs over the r-range 1.2–10 Å

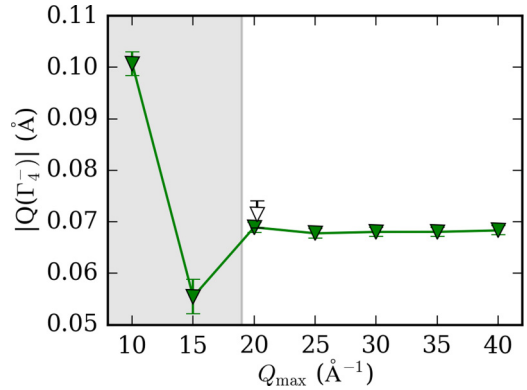

FIG. 4. Refined $|Q(\Gamma_4^-)|$ values for rhombohedrally constrained Ti and O distortions for a room-temperature $BaTiO_3$ PDF measured on GEM and processed with Q_{max} values ranging from 10 to 40 $Å^{-1}$ in steps of 5 $Å^{-1}$ (green filled markers). The unfilled marker represents the $|Q(\Gamma_4^-)|$ value for the lowest pressure [0.24(2) GPa], ambient temperature measurement of $BaTiO_3$ on PEARL.

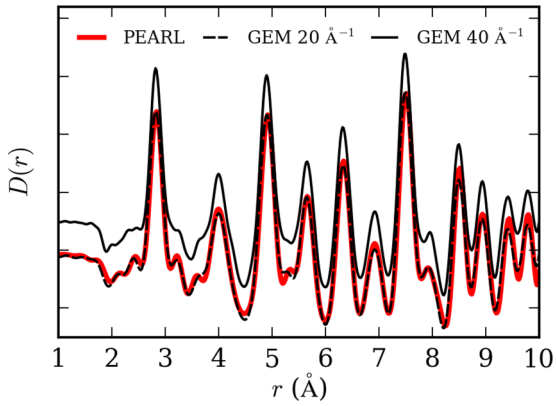

FIG. 5. PDFs of $BaTiO_3$ measured on PEARL at 0.24 GPa, processed with a Q_{max} of 20.32 Å^{-1}, and on GEM at ambient pressure and temperature, processed with Q_{max} values of 20 and 40 Å^{-1} (offset in the y-direction).

and the resulting $|Q(\Gamma_4^-)|$ values for Ti are shown in Fig. 4. They show notable consistency over the range 20–40 Å^{-1} and crucially, the values refined against our 0.24 GPa PEARL data with $Q_{max} = 20.32$ Å^{-1} are in excellent agreement, falling within error of each other. At $Q_{max} = 15$ Å^{-1} the values become inconsistent with those found for higher resolution PDFs. This establishes the lower limit in Q_{max} with respect to extracting physically meaningful displacements in this reported study and validates the sensitivity of the high-pressure PDFs with respect to the local-order parameters that we seek to probe. A 293 K total scattering measurement of $BaTiO_3$ on the GEM instrument provides a good comparison to the lowest pressure [0.24(2) GPa], ambient temperature PEARL measurement. Figure 5 shows that PDFs measured on GEM and PEARL (i.e., in a vanadium can and PE press, respectively) and processed with the same Q_{max} very closely agree, again, validating the high-pressure data.

[1] I. B. Bersuker, Phys. Lett. **20**, 589 (1966).
[2] M. Acosta, N. Novak, V. Rojas, S. Patel, R. Vaish, J. Koruza, G. A. Rossetti, and J. Rödel, Appl. Phys. Rev. **4**, 041305 (2017).
[3] A. V. Hippel, R. G. Breckenridge, F. G. Chesley, and L. Tisza, Ind. Eng. Chem. **38**, 1097 (1946).
[4] H. D. Megaw, Proc. R. Soc. London **189**, 261 (1947).
[5] W. Cochran, Adv. Phys. **9**, 387 (1960).
[6] S. A. Hayward and E. K. H. Salje, J. Phys.: Condens. Matter **14**, L599 (2002).
[7] R. Comés, M. Lambert, and A. Guinier, Solid State Commun. **6**, 715 (1968).
[8] S. Ravy, J.-P. Itié, A. Polian, and M. Hanfland, Phys. Rev. Lett. **99**, 117601 (2007).
[9] M. Paściak, T. R. Welberry, J. Kulda, S. Leoni, and J. Hlinka, Phys. Rev. Lett. **120**, 167601 (2018).
[10] A. M. Quittet and M. Lambert, Solid State Commun. **12**, 1053 (1973).
[11] B. Ravel, E. A. Stern, R. I. Vedrinskii, and V. Kraizman, Ferroelectrics **206**, 407 (1998).
[12] B. Zalar, V. V. Laguta, and R. Blinc, Phys. Rev. Lett. **90**, 037601 (2003).
[13] C. Laulhé, F. Hippert, R. Bellissent, A. Simon, and G. J. Cuello, Phys. Rev. B **79**, 064104 (2009).
[14] M. S. Senn, D. A. Keen, T. C. A. Lucas, J. A. Hriljac, and A. L. Goodwin, Phys. Rev. Lett. **116**, 207602 (2016).
[15] Y. Luspin, J. L. Servoin, and F. Gervais, J. Phys. C: Solid State Phys. **13**, 3761 (1980).
[16] J. Harada, J. D. Axe, and G. Shirane, Phys. Rev. B **4**, 155 (1971).
[17] Y. Yamada, G. Shirane, and A. Linz, Phys. Rev. **177**, 848 (1969).
[18] E. A. Stern, Phys. Rev. Lett. **93**, 037601 (2004).
[19] C. M. Culbertson, A. T. Flak, M. Yatskin, P. H. Cheong, D. P. Cann, and M. R. Dolgos, Sci. Rep. **10**, 3729 (2020).
[20] I. A. Kornev, L. Bellaiche, P. Bouvier, P. E. Janolin, B. Dkhil, and J. Kreisel, Phys. Rev. Lett. **95**, 196804 (2005).
[21] T. Ishidate, S. Abe, H. Takahashi, and N. Môri, Phys. Rev. Lett. **78**, 2397 (1997).
[22] C. L. Bull, C. J. Ridley, K. S. Knight, N. P. Funnell, and A. S. Gibbs, Materials Advances **2**, 6094 (2021).
[23] U. D. Venkateswaran, V. M. Naik, and R. Naik, Phys. Rev. B **58**, 14256 (1998).
[24] J. P. Itié, B. Couzinet, A. Polian, A. M. Flank, and P. Lagarde, Europhys. Lett. **74**, 706 (2006).
[25] L. Ehm, L. A. Borkowski, J. B. Parise, S. Ghose, and Z. Chen, Appl. Phys. Lett. **98**, 021901 (2011).
[26] H. Y. Playford, M. G. Tucker, and C. L. Bull, J. Appl. Crystallogr. **50**, 87 (2017).
[27] A. Herlihy, H. S. Geddes, G. C. Sosso, C. L. Bull, C. J. Ridley, A. L. Goodwin, M. S. Senn, and N. P. Funnell, J. Appl. Crystallogr. **54**, 1546 (2021).
[28] T. A. Bird, A. Herlihy, and M. S. Senn, J. Appl. Crystallogr. **54**, 1514 (2021).
[29] M. S. Senn, F. Pomiro, A. Herlihy, and N. P. Funnell, Local structure studies in the pressure-induced order-disorder phase transition of barium titanate, STFC ISIS Neutron and Muon Source, 2019, https://doi.org/10.5286/ISIS.E.RB1910162.
[30] C. L. Bull, N. P. Funnell, M. G. Tucker, S. Hull, D. J. Francis, and W. G. Marshall, High Press. Res. **36**, 493 (2016).
[31] S. Klotz, J. Philippe, C. L. Bull, J. S. Loveday, and R. J. Nelmes, High Press. Res. **33**, 214 (2013).
[32] O. Arnold, J. C. Bilheux, J. M. Borreguero, A. Buts, S. I. Campbell, L. Chapon, M. Doucet, N. Draper, R. Ferraz Leal, M. A. Gigg, V. E. Lynch, A. Markvardsen, D. J. Mikkelson, R. L. Mikkelson, R. Miller, K. Palmen, P. Parker, G. Passos, T. G. Perring, P. F. Peterson *et al.*, Nucl. Instrum. Methods Phys. Res., Sect. A **764**, 156 (2014).
[33] M. G. Tucker, D. A. Keen, M. T. Dove, A. L. Goodwin, and Q. Hui, J. Phys.: Condens. Matter **19**, 335218 (2007).
[34] A. A. Coelho, J. Appl. Crystallogr. **51**, 210 (2018).
[35] M. B. Smith, K. Page, T. Siegrist, P. L. Redmond, E. C. Walter, R. Seshadri, L. E. Brus, and M. L. Steigerwald, J. Am. Chem. Soc. **130**, 6955 (2008).

[36] T.-M. Usher, T. Iamsasri, and J. S. Forrester, J. Appl. Phys. **120**, 184102 (2016).
[37] D. Hou, C. Zhao, A. R. Paterson, S. Li, and J. L. Jones, J. Eur. Ceram. Soc. **38**, 971 (2018).
[38] See Supplemental Material at http://link.aps.org/supplemental/10.1103/PhysRevB.105.094114 for further details of modeling approaches and Rietveld refinements.
[39] B. J. Campbell, H. T. Stokes, D. E. Tanner, and D. M. Hatch, J. Appl. Crystallogr. **39**, 607 (2006).
[40] P. Pruzan, D. Gourdain, J. C. Chervin, B. Canny, B. Couzinet, and M. Hanfland, Solid State Commun. **123**, 21 (2002).
[41] B. K. Greve, K. L. Martin, P. L. Lee, P. J. Chupas, K. W. Chapman, and A. P. Wilkinson, J. Am. Chem. Soc. **132**, 15496 (2010).
[42] T. A. Bird, J. Woodland-Scott, L. Hu, M. T. Wharmby, J. Chen, A. L. Goodwin, and M. S. Senn, Phys. Rev. B **101**, 064306 (2020).
[43] K. W. Chapman, P. J. Chupas, R. Maxey, and J. W. Richardson, ChemComm. **38**, 4013 (2006).
[44] H. L. B. Boström, I. E. Collings, D. Daisenberger, C. J. Ridley, N. P. Funnell, and A. B. Cairns, J. Am. Chem. Soc. **143**, 3544 (2021).